A LiDAR-Based Method for Incorporating Foliar Biomass in Aboveground Carbon Estimates in Tropical Forest Enrichment Plantations

Stephane Takoudjou Momo *, Achille Biwole, Pauline - Andrée Medou Me Ze, Hermann Kondjio, Stephane Tchakoudeu, Yanick Serge Nkoulou, Bonaventure Sonké, Jean Louis Doucet

Posted Date: 25 May 2026

doi: 10.20944/preprints202603.1717.v2

Keywords: AGB allocation; LiDAR; allometry; tree architecture; tropical forest plantations; Congo Basin

 doi:10.20944/preprints202603.1717.v2

Article

A LiDAR-Based Method for Incorporating Foliar Biomass in Aboveground Carbon Estimates in Tropical Forest Enrichment Plantations

Stéphane Takoudjou Momo [1,2,3,*], Achille Biwolé [4], Pauline - Andrée Medou Me Ze [1,5], Hermann Kondjio [4], Stephane Tchakoudeu [5], Yanick Serge Nkoulou [6], Bonaventure Sonké [2] and Jean Louis Doucet [1]

[1] Forest Is Life, TERRA Teaching and Research Centre, Gembloux Agro-Bio Tech, University of Liège, Passage des Déportés 2, 5030 Gembloux, Belgium
[2] Plant Systematic and Ecology Laboratory (LaBosystE), Department of Biology, Higher Teachers' Training College, University of Yaoundé I, P.O. Box 047, Yaoundé, Cameroon
[3] Congo Basin institute, University of California, Los Angeles, Los Angeles, CA, USA
[4] Laboratory of Forest Resources and Wood Valorisation, Advanced Teacher's Training College for Technical Education, The University of Douala, P.O. Box. 1872, Douala, Cameroon
[5] Pallisco SARL, Avenue des Cocotiers 478, BP 394, Douala, Cameroon
[6] Association Technique Internationale des Bois Tropicaux, Cameroon
* Correspondence: takoudjoumomo@gmail.com

Abstract

Accurately quantifying aboveground biomass (AGB) in tropical forest enrichment plantations remains challenging, particularly in managed regenerating stands where tree crown architecture, size structure, and species composition differ from the datasets used to calibrate classical allometric equations. Here, we assess whether AGB in tropical forest enrichment plantations can be estimated more accurately by combining tree-specific woody volume reconstructed from mobile laser scanning (MLS) with an explicit foliar-biomass component. We combined destructive measurements from 83 trees with high-resolution MLS point clouds to quantify biomass components, calibrate leaf-mass models, and assess the contribution of foliage to total AGB. Stems accounted for most of the biomass (65%), whereas leaves contributed only 3% on average. Among the models tested, Model 3, which included DBH, projected crown area, and wood density, showed the best performance (R^2 = 54.4%; RMSE = 2.43 kg). The main gain relative to regional (-20.4%) and pantropical (-25.6%) allometric equations came from the use of MLS-derived woody volume combined with species wood density, whereas the inclusion of predicted leaf biomass provided a moderate additional correction to the remaining bias. These results highlight the importance of canopy structure for biomass estimation in enrichment plantations and managed regenerating stands and support the use of LiDAR data as a robust alternative for AGB assessment in this context.

Keywords: AGB allocation; LiDAR; allometry; tree architecture; tropical forest plantations; Congo Basin

1. Introduction

Tropical forests exhibit extraordinary structural and functional complexity, driven by the diversity of life forms and ecological processes they host [1,2]. Tree architecture, liana loads and multilayered understories make them not only among the most remarkable ecosystems on Earth, but also among the most ecologically important. They host over two-thirds of the planet's terrestrial biodiversity and play a central role in stabilizing global climate systems [3]. They constitute major carbon deposit, storing around 55% of all carbon contained in forest biomass, most of it in the

 doi:10.20944/preprints202603.1717.v2

aboveground compartments of trees [4–6]. Yet, despite their ecological importance, tropical forests are increasingly exposed to deforestation, degradation, and climate change [7–9]. Accurately quantifying their biomass has therefore become a major priority for forest monitoring, carbon accounting, and restoration planning [10,11].

For decades, aboveground biomass (AGB) has been estimated using allometric equations derived from destructive harvesting [12–14]. These equations typically relate diameter at breast height (DBH, cm), tree height (H, m), and wood density (WD) to AGB [14–19]. While widely used, these models have important limitations: they are often calibrated on restricted datasets, may not capture the structural diversity of tropical forests, and may be poorly transferable to planted or agroforestry systems where tree architecture differs from that of natural forests. Applying them broadly can therefore generate substantial biases [20–22] , especially in forests undergoing active regeneration or management [23,24]. Goodman et al. [21], for instance, showed that pantropical equations could underestimate AGB by up to 46% in dense tropical forests due to architectural variation. Similarly, previous studies have shown that crown architecture can cause substantial bias in biomass estimation [22,25]. These findings highlight the need for alternative or complementary predictors of AGB beyond DBH and height, particularly those that better capture crown structure [26]. Yet, destructive datasets specifically designed to validate such alternatives remain scarce.

Over the past decade, LiDAR has profoundly transformed forest ecology and biomass research [27]. Ground-based LiDAR technologies, including terrestrial laser scanning (TLS) and mobile laser scanning (MLS), now provide highly detailed three-dimensional descriptions of trees and forest stands [26,27]. Rather than relying solely on indirect proxies such as DBH, they capture the geometry of stems, branches, and crowns [27–30]. These data can be converted into quantitative structure models (QSMs), which estimate woody volume with unprecedented precision [31–36]. Combined with species-specific wood density values, QSMs can provide direct, non-destructive estimates of woody biomass [27,37,38] or support the development of new allometric equations [39–41]. In tropical forests, TLS-based estimates have shown strong agreement with destructive measurements [39,41–43]. Beyond tree-level applications, TLS and MLS also provide critical reference data for calibrating and validating large-scale spaceborne biomass products such as GEDI and BIOMASS [44,45].

However, most LiDAR-based biomass workflows remain strongly wood-centred. QSM-based approaches are primarily designed to reconstruct woody components, whereas leaves are often removed during processing because of their thin, overlapping, and highly irregular structure. As a result, most TLS- and MLS-based AGB estimates focus on stems and branches, implicitly treating the leafy compartment as secondary. Yet foliage remains ecologically important because it reflects crown architecture, light interception, and broader functional strategies, and because its relative contribution to total AGB may be higher in young trees and regenerating stands than in mature forests [16,46–48]. This distinction is important. The ecological relevance of leaves does not necessarily imply that they are the dominant source of improvement in total AGB estimation. In practice, the largest gain in LiDAR-based biomass estimation may come from replacing generic allometric predictions with tree-specific woody volume reconstructed from three-dimensional data, while the foliar component may provide a smaller, additional correction. Clarifying this balance is particularly important in enrichment plantations established within open secondary forests, where tree architecture and biomass allocation may differ from the contexts in which conventional allometries were calibrated. Although major efforts have been devoted to leaf/wood segmentation [49,50], the possibility of estimating leaf biomass from whole-crown structure rather than explicit segmentation remains largely unexplored.

Crown architecture provides a useful bridge between these two dimensions. Traits such as projected crown area, crown depth, and related crown-shape descriptors are linked to light interception, mechanical stability, and competitive strategy [26,30,51–54], and can be derived directly from 3D LiDAR data. However, despite their functional relevance, these crown attributes have rarely

 doi:10.20944/preprints202603.1717.v2

been evaluated as predictors of foliar biomass using paired destructive and LiDAR datasets [26,30,51–57].

Against this background, the main gap is not simply whether leaves matter ecologically, but whether a compartment-explicit LiDAR framework can improve AGB estimation in enrichment plantations by combining tree-specific woody volume with a measurable foliar component. We therefore ask two main questions: first, whether leaf biomass can be predicted from MLS-derived crown metrics; and second, whether incorporating this foliar term provides an additional gain once woody biomass has already been reconstructed from MLS-derived volume and wood density. We assess biomass partitioning among tree compartments, develop models of leaf biomass from crown structure and evaluate the extent to which this foliar component provides an additional gain from MLS-derived volume and wood density. More broadly, we expect this study to contribute to ongoing efforts to better connect structural remote-sensing measurements with the functional understanding of managed regenerating tropical forest systems, while recognizing that the present results were obtained in a specific enrichment-plantation context.

1. Materials and Methods

2.1. Study Area

The study was conducted in southeastern Cameroon, within forest management units (FMUs) 10-030, 10-042, and 10-044 managed by Pallisco-CIFM (Figure). The region belongs to the Guineo-Congolian semi-deciduous moist forest, dominated by species from Malvaceae and Cannabaceae [58,59]. The climate is equatorial with two rainy seasons, annual rainfall of 1,300-1,800 mm, and mean temperature ~24 °C [60]. Elevation ranges between 600-760 m on ferrallitic soils [61].

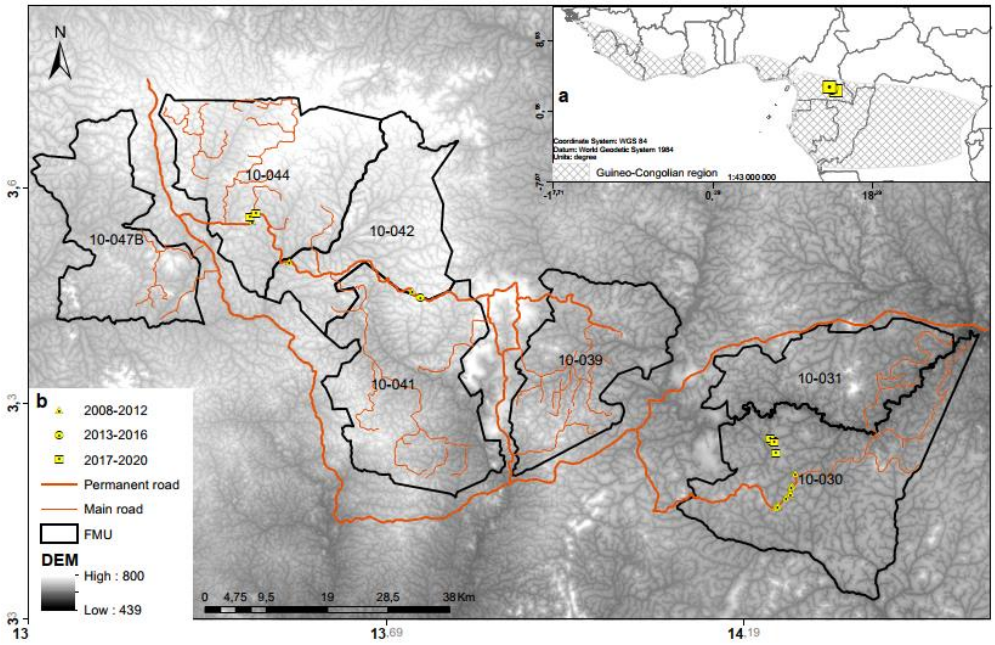

Figure 1. Map of the study area showing forest management units and sampled enrichment plantations in southeastern Cameroon.

Sampling was carried out in enrichment plantations established by Pallisco-CIFM as part of its regeneration program. These plantations were installed from 2008 onward within open secondary forests. After marking large-diameter trees (>60 cm DBH) and commercial species, the understorey was cleared either manually with machetes or mechanically with bulldozers. Nursery-grown seedlings of timber species were then planted at a spacing of 3 × 3 m, either in blocks of 25 seedlings (15 × 15 m) or along lines [62].

 doi:10.20944/preprints202603.1717.v2

2.2. Data Collection

2.2.1. LiDAR Acquisitions

Between December 2023 and January 2024, 19 plots ranging from 0.2 to 1.6 ha were surveyed using the handheld mobile laser scanner GeoSLAM ZEB-HORIZON (MLS) (see Appendix 1, Table I). This single-return instrument operates at 903 nm, records approximately 300,000 points s^{-1}, integrates 16 sensors [63,64], has a maximum range of 100 m, a nominal accuracy of 6 mm, and a field of view of 360° × 270° [63–65].

Before each acquisition, only light manual clearing was carried out to open a narrow walking paths between planted rows and blocks. This was necessary because most plantations were not regularly maintained and the understorey remained dense, often dominated by Marantaceae and other herbaceous vegetation typical of tropical secondary forests. The objective was primarily to facilitate operator movement and reduce severe near-ground occlusion, rather than to fully clear the understorey around sampled trees. Two white reference spheres were systematically placed at the plot origin to facilitate post-processing, including identification of the starting point and automatic alignment of the point cloud to geographic north. Unlike earlier MLS systems, the GeoSLAM ZEB-HORIZON performs co-registration during acquisition, producing a complete 3D point cloud at the end of each survey. Plots were selected to cover a range of plantation ages (4-15 years), planting configurations (block vs. row planting), and site preparation methods (manual vs. bulldozer-assisted clearing) (see Appendix 1, Table I).

1.2.2. Destructive Sampling

Between March and May 2024, 83 trees belonging to 9 species across 6 families were destructively sampled across previously scanned plantation plots (Table). These species covered a wide range of structural and functional strategies, including pioneers (P) as well as non-pioneer light-demanding (NPLD) guilds.

Table 1. Families, species, and main characteristics of destructively sampled trees, including scientific and commercial names, sample size (n), diameter range (DBH, cm), mean wood density (WD, g cm^{-3}), and ecological guild.

Family	Genus	Species	Com. name	n	DBH	H	WD	Guild
Combretaceae	Terminalia	superba	Fraké	18	[6.7-33.9]	[4.55-22.36]	0.459	P
Fabaceae	Bobgunnia	fistuloides	Pao rosa	7	[5.2-22]	[6.33-16.5]	0.866	P
	Cylicodiscus	gabunensis	Okan	6	[5.9-14]	[4.41-9.16]	0.79	P
	Pterocarpus	soyauxii	Padouk	3	[5.9-8.6]	[4.11-7.1]	0.658	NPLD
Malvaceae	Mansonia	altissima	Bété	12	[5.9-23]	[6.62-15.1]	0.564	
	Triplochiton	scleroxylon	Ayous	15	[5.7-30.7]	[5.06-24.63]	0.334	P
Meliaceae	Entandrophragma	utile	Sipo	6	[5.2-9]	[4.91-6.69]	0.537	NPLD
Ochnaceae	Lophira	alata	Azobé	8	[8.1-32]	[7.13-14.27]	0.897	P
Sapotaceae	Baillonella	toxisperma	Moabi	8	[5.5-13]	[5.2-11.04]	0.725	NPLD

Sample size ranged from 6 to 17 individuals per species, with DBH values between 3.76 and 34.26 cm and total heights between 4.1 and 22.4 m. Because sample size varied among species, the dataset was not balanced across taxa. In addition, wood density (WD) was assigned at the species level from the Global Wood Density Database rather than measured individually for each tree [66,67].

Before felling, diameter at breast height (DBH) was measured at 1.3 m above ground, or above the last stem irregularity when necessary, and total tree height was determined using a Haglöf Vertex V hypsometer [16]. After felling, each tree was divided into three vertical compartments: (1) the stump, corresponding to the portion of the stem below the felling cut; (2) the stem, corresponding to the merchantable bole; and (3) the crown, including all living branches and foliage above the main stem.

Stem and stump volumes were estimated by sectional cubing. The bole was divided into successive 1-m logs from the stump to the base of the live crown, and the last segment was measured

 doi:10.20944/preprints202603.1717.v2

up to the first major branch insertion to ensure complete coverage of the merchantable stem [16]. For each log i, the over-bark diameters at the lower and upper ends (D_{1i} and D_{2i}, in cm) were measured using a diameter tape, and log length (L_i, in m) was measured with a measuring tape. The volume of each log was then calculated using Smalian's formula (1):

$$V_i = \frac{\pi}{8} \times L_i(D_{1i}^2 + D_{2i}^2) \quad (1)$$

where diameters were converted from centimetres to metres before calculation, and V_i is expressed in cubic metres. Total stem volume was then obtained as (2):

$$V_{stem} = \sum_{i=1}^{n} V_i \quad (2)$$

Stump volume was calculated in the same way, treating the stump as an additional short log between ground level and the felling cut.

Fresh leaves and twigs $\leq$ 1cm in diameter were weighed in the field using an electronic balance (0.01 g precision), and subsamples were stored in airtight bags for laboratory analyses. Subsamples were oven-dried at 60 °C and reweighed until constant mass was reached (<1% variation between two weighings separated by 6 h), following Sirri et al. [68]. Total tree leaf mass (TLM, kg), used here as dry foliar biomass, was estimated by correcting fresh leaf mass with the species-specific mean moisture content (3).

$$TLM_{i,j} = FLM_{i,j} \times \left(1 - \frac{MC_j}{100}\right) \quad (3)$$

where, $FLM_{i,j}$ is fresh leaf mass of individual i of species j, MC_j is the mean moisture content of species j, calculated from all available subsamples for that species as: $MC_j = \frac{1}{n}\sum_{i=1}^{n}(\frac{FMs_{i,j} - DMs_{i,j}}{FMs_{i,j}} \times 100)$ (4) where $DMs_{i,j}$ and $FMs_{i,j}$ are the dry and fresh subsample mass, respectively. We assume that within-species variation in MC is smaller than between-species and that a species-level mean provides a reasonable correction at the tree level.

Stump and stem volume were converted to biomass (AGB, in kg) using a species-level WD (g.cm^{-3}) values from the Global Wood Density Database [66,67]. The resulting stump and stem biomass (AGB_{ss}) were then combined with $TLM_{i,j}$ to obtain the destructively derived tree aboveground biomass (AGB_{Dest}).

1.2.2. LiDAR Point Cloud Processing and Structural Attribute Extraction

After automatic co-registration in the GeoSLAM software [43], individual trees were extracted from the plot point clouds using the semi-automatic workflow described by Martin-Ducup et al. [69]. This workflow (Appendix 2, Figure 1) involved: (i) matching field inventory records with the point cloud, (ii) isolating individual tree point clouds, and (iii) separating wood and leaf points using LeWoS [50]. Structural attributes, including DBH, total height, and crown metrics such as projected crown area (PCA, m²), were then extracted from each individual tree point cloud using the ITSMe R package [28] (Figure).

 doi:10.20944/preprints202603.1717.v2

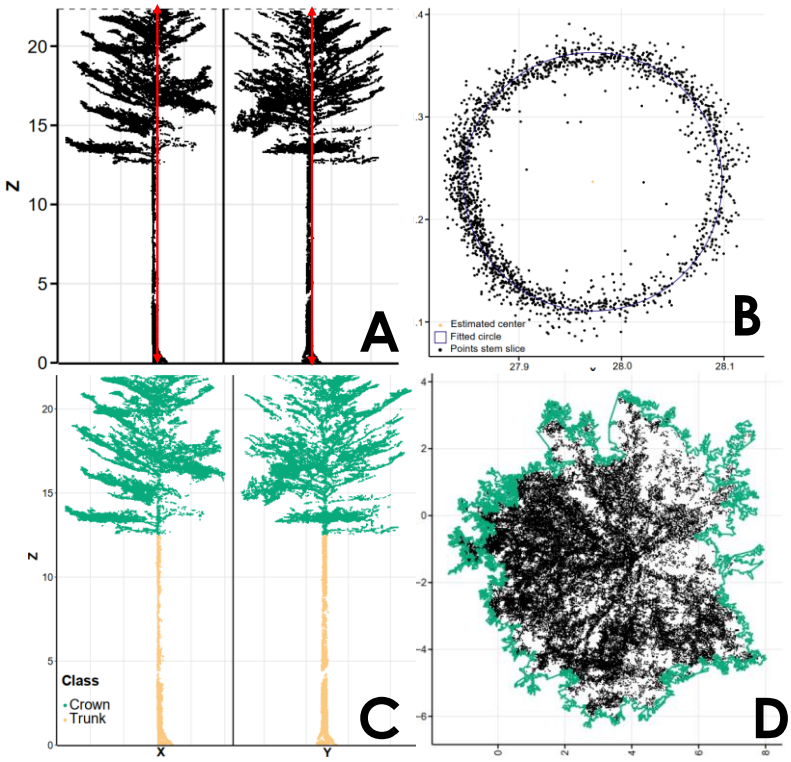

Figure 2. Workflow illustrating the extraction of structural and crown metrics from individual tree point clouds. (A) Tree height measurement. (B) Diameter at breast height estimated by fitting a circle to the stem cross-section. (C) Separation of trunk and crown components. (D) Projected crown area obtained from the horizontal projection of crown points onto the ground plane.

TreeQSM [29] was subsequently applied to the woody point clouds to reconstruct the woody structure and estimate woody volume. For each tree, the optimal QSM was retained based on its coherence with the original woody point cloud, including stem continuity, realistic branching topology, and the absence of obvious cylinder misplacement or over-segmentation. The retained QSM was then visually inspected in AMAPstudio-Scan, where manual refinement was restricted to correcting clearly misplaced cylinders under direct control of the original point cloud (https://amapstudio.cirad.fr/soft/scan/start). This step did not involve re-modelling the tree or altering its observed geometry; rather, it served as a constrained quality-control procedure to remove obvious reconstruction artefacts before volume extraction (see Momo Takoudjou et al.[39], for more details). Finally, MLS-derived aboveground biomass (AGB_{MLS}) was obtained by converting QSM volume into biomass using species-level WD values from Global Wood Density Database, accessed through the Biomass R package [66,67].

2.3. Data Analysis

Preliminary analyses included descriptive statistics and distribution checks for all structural and biomass variables. Relationships between destructively measured parameters (leaf mass, total AGB) and LiDAR-derived metrics were assessed using Pearson's correlation coefficients. Because stem, branch, and leaf biomass are constrained components of a common total AGB, biomass partitioning was analysed as compositional data at the individual-tree level. For each tree, the biomass of the three compartments was converted into proportions summing to one (5).

$$P_{i,j} = \frac{C_{i,j}}{AGB_j} \quad (5)$$

 doi:10.20944/preprints202603.1717.v2

where $P_{i,j}$ is the proportion of compartment i in tree j, C_{ij} is the biomass of compartment i in tree j, and AGB_j is the total AGB of tree j.

These proportions were transformed using isometric log-ratio (ilr) coordinates to account for the structural dependence among compartments. Species, DBH-class, and functional-guild effects on biomass partitioning were then tested using MANOVA on the transformed coordinates. For descriptive purposes, an aggregated species × compartment heatmap was retained to visualize deviations from the overall mean allocation pattern.

Several structural predictors were initially explored for leaf-biomass modelling, including DBH, projected crown area (PCA), crown depth (CrD), and the height-to-diameter ratio (H/D). Preliminary model screening showed that CrD and H/D did not improve predictive performance relative to models based on DBH and PCA. We therefore retained a final set of three nested log–log models:

$$\text{m1}: \ln(TLM) \sim \beta_1 + \alpha_1 \times \ln(DBH) + \varepsilon \quad (6)$$

$$m2: \ln(TLM) \sim \beta_2 + \alpha_1 \times \ln(DBH) + \alpha_2 \times \ln(PCA) + \varepsilon \quad (7)$$

$$\text{m3}: \ln(TLM) \sim \beta_3 + \alpha_1 \times \ln(DBH) + \alpha_2 \times \ln(PCA) + \alpha_3 \times \ln(W) + \varepsilon \quad (8)$$

where, TLM (kg) is destructively measured leaf biomass, DBH is the diameter of breast height (cm), PCA is the projected crown area (m^2) and WD is species-level wood density, and β and α are the model coefficients, and ε is the residual error term, assumed to follow a normal distribution.

Because WD was available only at the species level, its effect should be interpreted as capturing both functional information and part of the taxonomic structure embedded in the sample. Models were compared using Akaike's Information Criterion (AIC), the coefficient of determination (R^2), and residual standard error (RSE). Predictive accuracy was evaluated using root mean square error (RMSE):

$$RMSE = \sqrt{1/n \sum_{i=1}^{n} \left(TLM_i - TLM_{ip}\right)^2} \quad (9)$$

where TLM_i and TLM_{ip} denote the observed and predicted values of total leaf biomass, respectively.

Because log-transformation introduces back-transformation bias, a correction factor was applied as CF = exp (RSE²/2), where RSE represents the residual standard error of the model [14,16]. Model robustness was assessed using two complementary cross-validation strategies [70]. Tree-level cross-validation evaluated predictive stability among individual trees by repeatedly withholding observations from the calibration dataset and predicting them from the remaining sample. Species-level cross-validation was used to assess transferability across taxa by testing model performance when predictions were evaluated across species rather than only across individuals. This distinction allowed us to separate within-sample predictive robustness from between-species generalization. Finally, MLS-derived AGB including foliage ($AGB_{MLSLeaf}$) was compared with MLS-derived woody AGB without foliage (AGB_{MLS}), destructive AGB, and two reference allometric models: the regional equation of Fayolle et al. [16] and the pantropical equation of Chave et al. [14]. Agreement with the destructive reference (AGB_{obs}) was quantified using bias (B, %) and relative error (S, %):

$$B = \left((\bar{\hat{y}} - \bar{y})/\bar{y}\right) \times 100 \quad (10)$$

where $\bar{\hat{y}}$ and $\bar{y}$ are average of predicted and observed AGB values.

$$S = \left((\hat{y} - y)/y\right) \times 100 \quad (11)$$

where $\hat{y}$ and y are of predicted and observed AGB values. Because the objective of this study was to compare the performance of alternative AGB estimation workflows, uncertainty was assessed comparatively through bias, RMSE, and relative error, rather than through full error propagation across all destructive and LiDAR-derived processing steps. All analyses were conducted in R (*version 4.5.0*, [71], with an alpha risk level of 0.05 for statistical significance.

 doi:10.20944/preprints202603.1717.v2

3. Results

3.1. Leaf Mass Contribution to Total Aboveground Biomass

Across the full dataset (n=83), tree-level compositional analysis confirmed that biomass partitioning among stem, branch, and leaf compartments differed significantly among species (Pillai's trace = 0.414, approx. F (16,148) =2.413, p=*0.003*). Biomass partitioning also varied significantly across DBH classes (Pillai's trace = 0.442, approx. F (6,158) =7.463, p<*0.001*), whereas no significant effect of functional guild was detected (Pillai's trace = 0.049, approx. F (2,80) =2.073, p=*0.133*). For descriptive purposes, Figure A highlights the species–compartment combinations that deviate most from the overall mean allocation pattern. At the species level, Entandrophragma utile showed the highest mean stem contribution (0.8) and the lowest branch contribution (0.133), whereas *Triplochiton scleroxylon* showed the lowest mean stem contribution (0.519) and the highest branch contribution (0.430). Mean leaf contribution remained low across species, ranging from 0.034 in *Mansonia altissima* to 0.067 in *Entandrophragma utile*. The species-level barplot presented in Appendix 3 (Figure 3) shows the same general pattern: stems consistently accounted for the largest share of AGB (approximately 60–80%), branches contributed about 20–40%, and leaves remained a minor component (<7%). Partitioning across DBH classes followed a similar gradient (Figure B): small trees (<10 cm DBH) showed lower stem contribution and proportionally higher branch and leaf fractions, whereas larger trees (>30 cm DBH) invested more strongly in the stem compartment. By contrast, differences between non-pioneer light-demanding and pioneer species remained modest, consistent with the non-significant guild effect detected by the compositional MANOVA (Appendix 3, Figure 3).

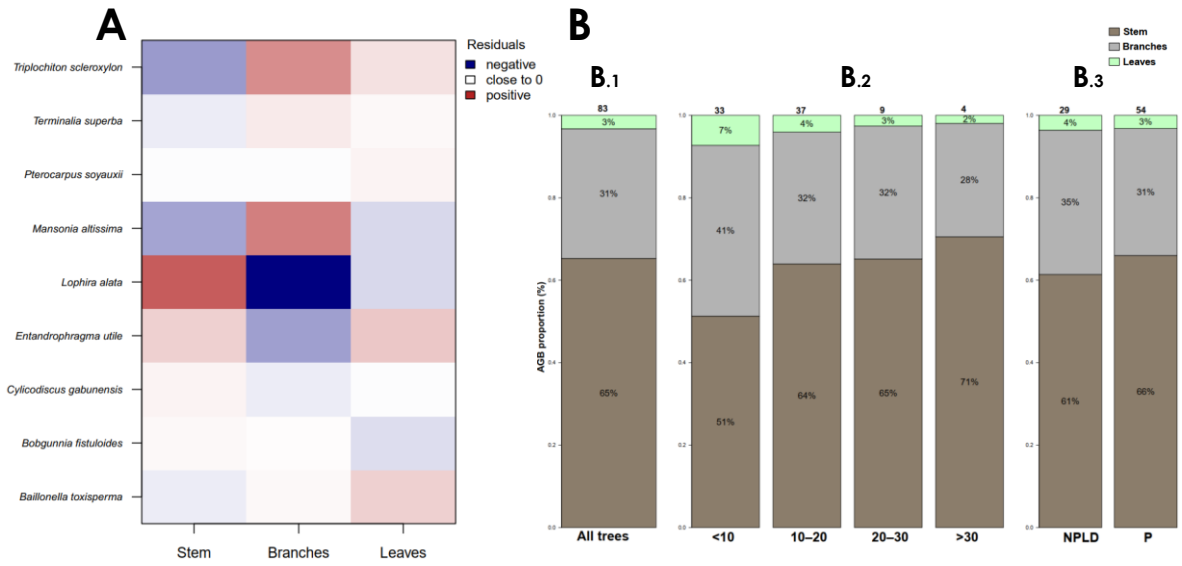

Figure 3. Partitioning of aboveground biomass among tree compartments. (A) Descriptive heatmap of species-level deviations in biomass allocation, based on aggregated Pearson residuals from a species × compartment table. Colours indicate the sign and magnitude of deviations from the overall mean allocation pattern. Statistical inference on biomass partitioning was performed separately using tree-level compositional MANOVA. (B) Relative contribution of tree compartments to total aboveground biomass for (B1) the full dataset, (B2) diameter classes, and (B3) functional guilds (NPLD and P). Numbers above bars indicate sample size.

3.1. Model Calibration and Validation Based on MLS Metrics

Among the three log-log models calibrated to predict total leaf mass (TLM), the DBH-only model showed the weakest performance (Table). It explained 48.2% of the observed variance, but residual and prediction errors remained relatively high (RSE = 0.83; RMSE = 2.77 kg). Adding projected crown area (PCA) improved model fit, increased explained variance to 52.5%, and slightly reduced AIC and RMSE. The full model, which includes DBH, PCA, and wood density (WD), provided the best fit to

 doi:10.20944/preprints202603.1717.v2

the destructive data, with the highest explained variance (R^2 = 54.4%) and the lowest AIC (173.96) and RMSE (2.43 kg).

Table 2. Log–log linear models developed to predict tree leaf dry mass (TLM, kg) from LiDAR-derived structural predictors. Explanatory variables included diameter at breast height (DBH, cm), projected crown area (PCA, m^2), and wood density (WD, g cm^{-3}). Parameter estimates (β, α_1, α_2, α_3) are reported with their standard errors (±SE), together with model fit and predictive performance metrics (R^2, RSE, AIC, RMSE). Significance levels are indicated by asterisks (*** $p < 0.001$, ** $p < 0.01$, * $p < 0.05$).

Models	Model Parameters				Model Performance			
	β (±)	α_1(±)	α_2(±)	α_3(±)	R^2	RSE	AIC	RMSE
m1: ln(TLM)~β + α_1× ln(DBH)	-2.96*** (0.46)	1.53*** (0.19)	-	-	48.19	0.78	179.4	2.6
m2: ln(TLM)~β + α_2× ln(PCA)	-2.67*** (0.45)	1.12*** (0.24)	0.32* (0.12)	-	52.52	0.75	174.9	2.5
m3: ln(TLM)~β + α_1× ln(DBH) + α_2× ln(PCA) + α_3× ln(WD)	-2.57*** (0.45)	1.15*** (0.24)	0.36** (0.12)	0.48. (0.28)	54.37	0.74	173.9	2.4

Despite this improvement, model performance remained moderate overall, with slightly more than half of the variance in TLM explained by the retained predictors. The selected model should therefore be interpreted as a useful but imperfect approximation of foliar biomass variation in this dataset, rather than as a highly precise predictor.

Cross-validation supported the relative stability of the three models (Figure). At the tree level, RMSE values ranged from 2.68 to 2.82 kg, indicating limited variation in predictive performance among models. At the species level, RMSE values were of similar magnitude, suggesting no substantial deterioration in prediction when validation was evaluated across taxa rather than across individuals. Nonetheless, the magnitude of these errors confirms that uncertainty in TLM prediction remains non-negligible, even for the best-performing model.

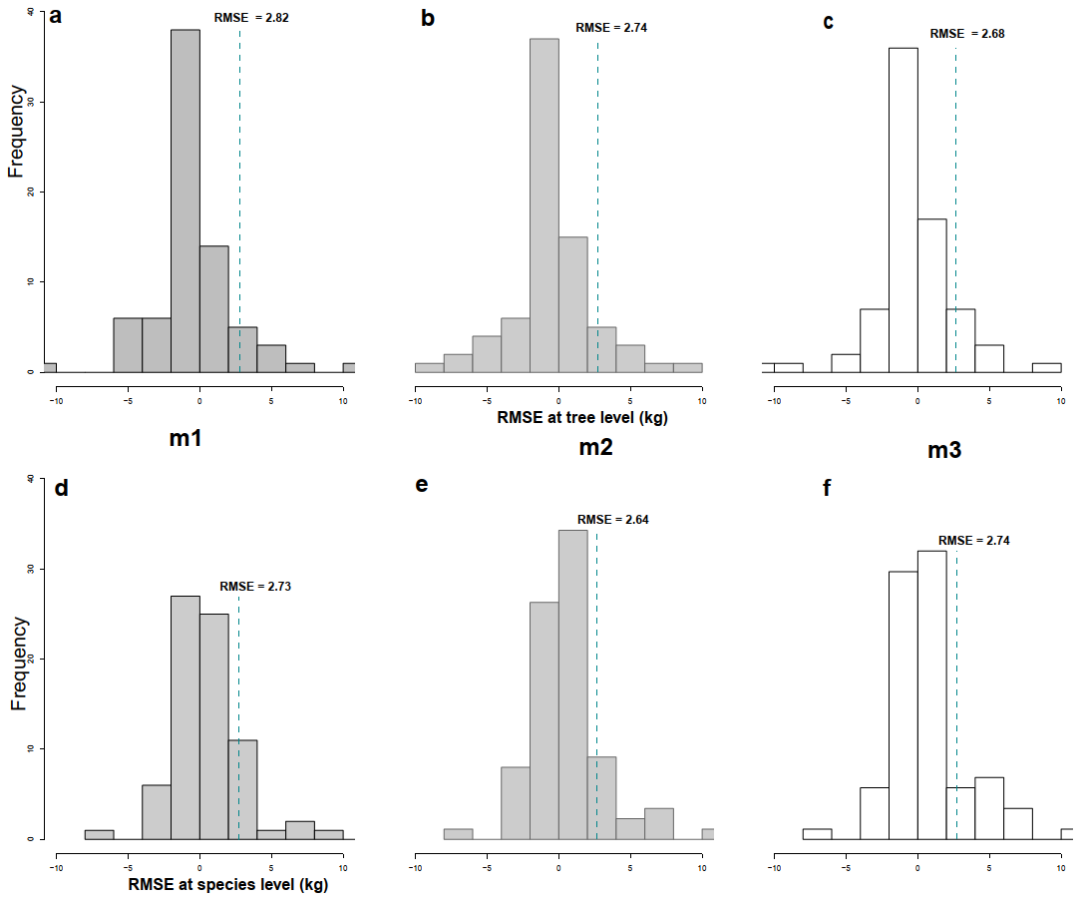

 doi:10.20944/preprints202603.1717.v2

Figure 4. Distribution of RMSE values (kg) for the three leaf-dry-mass models obtained by cross-validation at the tree (a-c) and species (d-f) levels. Vertical dashed lines show mean values of the RMSE.

3.1. Tree Level Biomass Estimations

Based on the cross-validation performance, Model 3 was selected to predict total leaf mass (TLM). These predictions were then added to MLS-derived woody biomass estimates to obtain $AGB_{MLSLeaf}$. Across all comparisons, the dominant improvement relative to classical allometric equations came from the use of tree-specific woody volume reconstructed from MLS and converted with species wood density. The explicit foliar component provided a smaller additional correction to the remaining discrepancy between MLS-derived and destructive AGB estimates. For MLS-based estimates alone, woody biomass excluding leaves was already close to the destructive reference (Bias = -2%). Adding predicted leaf mass shifted the bias to +1.91% (Figure a), indicating a relatively modest change in absolute terms. By contrast, the differences relative to conventional allometric equations were much larger. The regional model of Fayolle et al. [16] showed a strong negative bias (-20.38%; Figure b) and the pantropical model of Chave et al. [14], showed an even larger underestimation (-25.64%; Figure c). In both cases, MLS-derived estimates were substantially closer to the destructive reference than the allometric predictions.

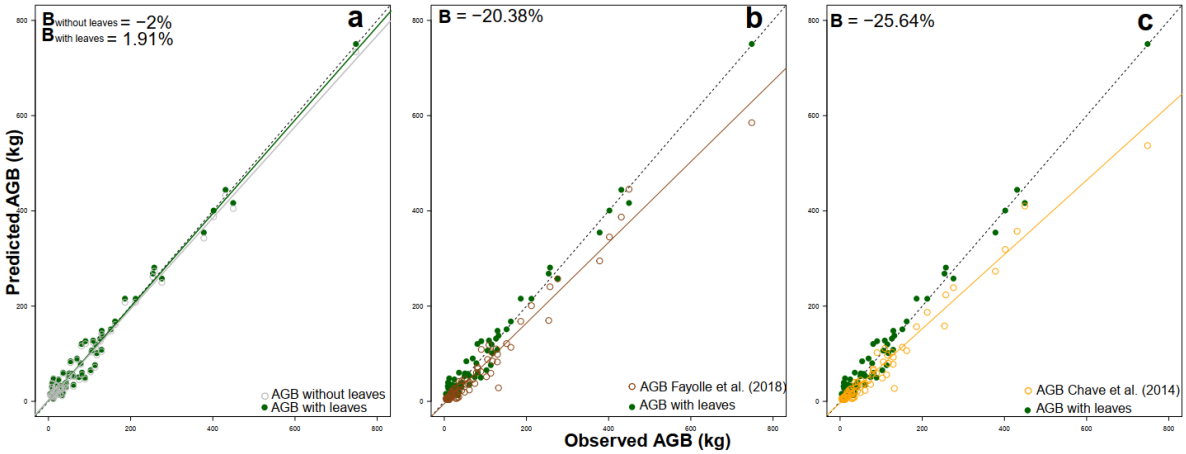

Figure 5. Relationship between observed aboveground biomass (AGB, kg) and estimates derived from MLS and reference allometric models. **(a)** Comparison of MLS-based AGB estimates obtained without and with leaf biomass. **(b)** Comparison between MLS-based AGB including leaf biomass and the regional allometric model of Fayolle et al. [16]. **(c)** Comparison between MLS-based AGB including leaf biomass and the pantropical model of Chave et al. [14]. The black dashed line indicates the 1:1 relationship, solid-coloured lines represent fitted regressions, and bias values are reported in the upper-left corner of each panel.

Given that the accuracy of AGB predictions can be strongly size-dependent, we explored how relative errors (S in %) behave across our DBH spectrum. Relative error also varied along the DBH gradient (Figure). For small trees (<8 cm DBH), MLS-based estimates tended to overestimate AGB, whereas the Chave et al. [14]equation consistently underestimated it. For intermediate diameters (10-30 cm), MLS-derived estimates remained close to zero error, while allometric predictions remained strongly negative, typically between -20% and -40%. For larger trees, errors converged somewhat, but MLS estimates remained closer to zero than the allometric models throughout most of the observed diameter range.

These comparisons should be interpreted within the specific context of enrichment plantations established in open secondary forests, where tree architecture and biomass allocation may differ from those of mature natural forests.

 doi:10.20944/preprints202603.1717.v2

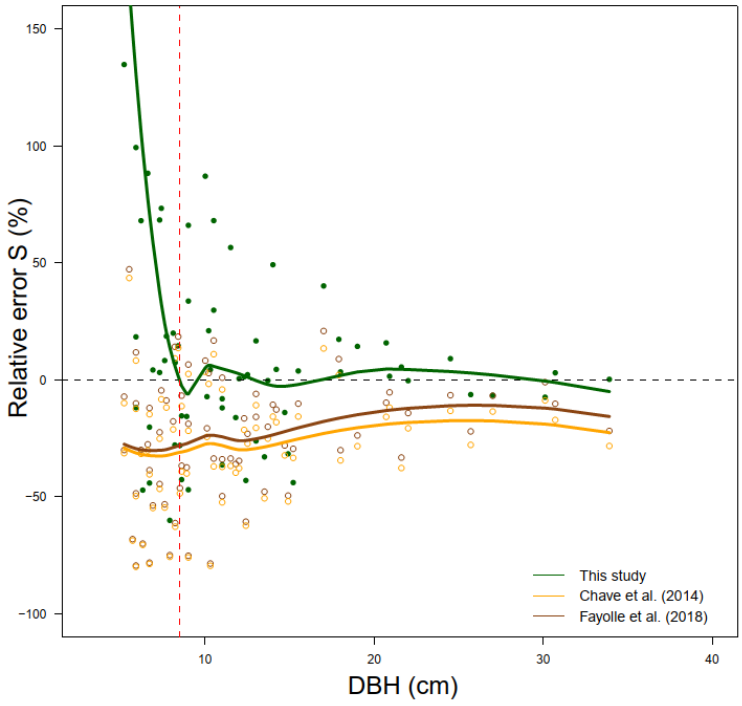

Figure 6. DBH-dependent relative error (S, %) in AGB predictions for MLS-derived estimates and the allometric models of Chave et al. [14]and Fayolle et al. [16].

3. Discussion

4.1. Foliar Biomass to Tropical AGB and Implications for Forest Structure

Our results show that foliar biomass represents a small fraction of total aboveground biomass (AGB), averaging about 3% across species and diameter classes. Although this proportion is modest compared to woody compartments, this range is consistent with previous destructive studies reporting leaf contributions between 2% and 15%, depending on species, stand type, and tree size [46–48]. In our dataset, leaf allocation declined with tree size, with small trees (<10 cm DBH) showing proportionally greater investment in crown components than larger individuals. This pattern is consistent with the general expectation that young trees invest more in light capture, whereas larger trees allocate more biomass to stem support and mechanical stability [24,72].

Species differences in biomass partitioning were significant, whereas differences between pioneer and non-pioneer light-demanding guilds were not. This suggests that variation among species is more pronounced than the broad guild contrast considered here, at least in this plantation context. At the same time, the consistently low leaf fraction across taxa indicates that foliage remains a secondary biomass compartment in absolute terms, even when it is functionally important. An additional source of uncertainty concerns the estimation of destructive foliar biomass itself. Total dry leaf mass was derived from fresh mass corrected using a species-level mean moisture content. Although operationally reasonable, this approach may mask within-species variation associated with crown position, tree size, microenvironment, or leaf age. Part of the residual variation in the foliar-biomass models may therefore reflect uncertainty introduced at the measurement stage rather than only biological variation in crown structure.

4.2. Performance of LiDAR-Derived Models for Predicting Foliar Mass and Improving AGB Estimates

Crown-based LiDAR metrics improved the prediction of total leaf mass (TLM), but model performance remained moderate. DBH alone explained about 48% of the observed variance, and the addition of projected crown area (PCA) and wood density (WD) improved fit only incrementally.

 doi:10.20944/preprints202603.1717.v2

The best-performing model combined DBH, PCA, and WD, but still explained only about 54% of TLM variation. This indicates that the model is useful for capturing broad patterns in foliar biomass, but not sufficiently precise to eliminate substantial residual uncertainty. These findings reinforce the idea that crown geometry rather than stem size alone captures key functional and structural determinants of leaf biomass [26,54].

The additional improvement achieved by including wood density (WD) highlights the importance of integrating species-specific functional traits into LiDAR-based biomass models [73]. This contribution of WD should also be interpreted cautiously. In this study, WD was assigned at the species level rather than measured for each tree, and species were unevenly represented in the sample. As a result, part of the apparent gain associated with WD may reflect taxonomic structure embedded in the dataset, rather than a fully general relationship between crown structure and leaf biomass. This does not invalidate the model in the present study system, but it does limit the extent to which the fitted coefficients can be interpreted as broadly transferable.

Cross-validation nevertheless showed that model performance was relatively stable across both tree-level and species-level partitions. RMSE values were of similar magnitude across validation schemes, suggesting limited overfitting and reasonable internal robustness. However, this stability should not be interpreted as evidence of high predictive precision; rather, it indicates that the fitted relationships remain broadly consistent within the range of species, sizes, and plantation with similar conditions. Few tropical studies have performed such rigorous validation on destructively sampled datasets, which strengthens the reliability of our approach [21,40,74]. A central result of this study is that the main improvement relative to regional and pantropical allometries comes from replacing generic biomass equations with tree-specific woody volume reconstructed from MLS and converted using species wood density. In that respect, MLS-based AGB without leaves was already close to the destructive reference, with a bias of about -2%. Adding a modelled foliar term did not fundamentally change the ranking of approaches but provided a modest secondary refinement by shifting the remaining bias to +1.9%. This distinction is important. Our results do not suggest that foliar biomass is the dominant reason why MLS-based estimates outperform classical allometries in this plantation context. Rather, they show that once woody biomass has been reconstructed directly from LiDAR-derived tree geometry, explicitly accounting for foliage can further improve total AGB estimates, especially in small trees and young stands where leaf contribution is proportionally higher. In other words, foliage should be viewed as a refinement of an already improved volumetric framework, not as the primary driver of the gain relative to conventional allometries. When compared with the equations of Fayolle et al. [16] and Chave et al. [14], MLS-derived estimates were substantially closer to destructive AGB. This confirms that generic allometric equations may underperform in enrichment plantations established within open secondary forests, where architecture and biomass allocation can differ from the calibration domain of natural-forest allometries. Importantly, most existing TLS/MLS-based AGB studies still ignore foliage even in tropical forests, assuming its contribution to be negligible [38,39,41,75]. Future work should therefore focus on three priorities: improving foliar-biomass prediction, testing the framework under more diverse forest conditions, and propagating uncertainty more explicitly across destructive measurements, moisture correction, species-level WD assignment, and QSM-based volume reconstruction algorithms.

4.3. DBH-Dependent Errors

Size-dependent error analysis helps explain why MLS-based estimates and classical allometries diverged most strongly in small and intermediate trees. For small trees (< 8cm of DBH), MLS tended to overestimate AGB while allometries strongly underestimated it. This likely reflects both the weak calibration of many allometric equations for small stems [14,16] and the relatively greater contribution of crown architecture at early growth stages [24,72,76]. In contrast, MLS directly captures the three-dimensional structure of stems and crowns, even when DBH alone is a weak proxy for total aboveground structure [27,77,78]. For intermediate trees (10-30 cm DBH), MLS-derived estimates were close to zero error, while allometric predictions remained consistently negative. This

 doi:10.20944/preprints202603.1717.v2

suggests that direct structural reconstruction is particularly informative in the size range that dominates many enrichment plantations. For larger trees, errors became more similar across approaches, but MLS estimates remained closer to zero across most of the observed DBH range [79]. This has major implications for carbon accounting, forest restoration monitoring, and REDD+ programs, which critically depend on accurate AGB estimation [44,80]. Beyond improving model fit, these results support the view that direct volumetric reconstruction is especially valuable in structurally heterogeneous plantation and regenerating-forest settings. They also show that the contribution of foliage is not uniform across the size gradient: although modest in absolute terms, it becomes more relevant in the smaller trees for which leaf and crown fractions are proportionally larger. Even so, the principal gain in predictive accuracy remains associated with MLS-derived woody volume, while foliar biomass provides a secondary improvement layered onto that framework.

Conclusion

Our study shows that the main improvement in AGB estimation in tropical forest enrichment plantations comes from replacing generic allometric predictions with woody biomass reconstructed from MLS-derived tree volume and species wood density. LiDAR-derived AGB was nearly unbiased across most of the diameter range, whereas classical allometries exhibited persistent negative errors linked to their inability to characterize crown structure and species-specific allocation strategies. Beyond this, our results reveal clear size-dependent deviations that help explain the long-recognized mismatch between direct structural approaches and pantropical or regional allometries. These findings highlight the importance of canopy architecture as a driver of biomass variation in managed regenerating stands. They also show that leaf biomass, although quantitatively small, is not constant across species and size classes and can provide a meaningful additional correction when woody biomass has already been estimated directly from LiDAR-derived structure. More broadly, this study helps bridge the gap between destructive and LiDAR-based biomass assessment by showing that a compartment-explicit approach can improve AGB estimation in enrichment plantations established within open secondary forests. It supports the use of LiDAR for biomass monitoring in enrichment plantations, restoration stands, and comparable managed regenerating forests, while broader extrapolation to tropical forests in general should remain cautious.

Supplementary Materials: The following supporting information can be downloaded at the website of this paper posted on Preprints.org.

Acknowledgments: This research was made possible with the support of the Applied Research in Ecology and Social Sciences in Support of the Sustainable Management of Forest Ecosystems in Central Africa (RESSAC) program implemented by CIFOR-ICRAF, and with the financial assistance of the European Union. We are also grateful to Philippe Lejeune, Jean-Yves De Vleeschouwer, direction and staff of Pallisco company, especially Richard Fétéke and all their support during field missions.

Conflicts of Interest: The authors declare no conflicts of interest.

Author Contributions: Conceptualization S.T.M., P.A.M.M.Z. and A.B.; formal analysis, S.T.M.; investigation, S.T.M., P.A.M.M.Z., ST. and A.B.; data curation, S.T.M., P.A.M.M.Z., H.K., Y.S.N., and A.B.; writing original draft, S.T.M., A.B., BS. and J.L.D. All authors have read and agreed to the published version of the manuscript.

Data Availability Statement: Requests for data and materials should be addressed to the first author at takoudjoumomo@gmail.com.

References

1. Hallé, Francis.; Oldeman, R.A.A.; Tomlinson, P.B. *Tropical Trees and Forests : An Architectural Analysis*; Springer Berlin Heidelberg, 1978; ISBN 3642811906.

 doi:10.20944/preprints202603.1717.v2

2. Poorter, L.; Bongers, L.; Bongers, F. Architecture of 54 Moist-Forest Tree Species: Traits, Trade-Offs, and Functional Groups. *Ecology* **2006**, *87*, 1289–1301, doi:10.1890/0012-9658(2006)87[1289:AOMTST]2.0.CO;2.
3. Bonan, G.B. Forests and Climate Change: Forcings, Feedbacks, and the Climate Benefits of Forests. *Science (1979).* **2008**, *320*, 1444–1449, doi:10.1126/science.1155121.
4. Bastin, J.-F.; Rutishauser, E.; Kellner, J.R.; Saatchi, S.; Pélissier, R.; Hérault, B.; Slik, F.; Bogaert, J.; De Cannière, C.; Marshall, A.R.; et al. Pan-Tropical Prediction of Forest Structure from the Largest Trees. *Global Ecology and Biogeography* **2018**, 1–18, doi:10.1111/geb.12803.
5. Hubau, W.; Lewis, S.L.; Phillips, O.L.; Affum-Baffoe, K.; Beeckman, H.; Cuní-Sanchez, A.; Daniels, A.K.; Ewango, C.E.N.; Fauset, S.; Mukinzi, J.M.; et al. Asynchronous Carbon Sink Saturation in African and Amazonian Tropical Forests. *Nature* **2020**, *579*, 80–87, doi:10.1038/s41586-020-2035-0.
6. Pan, Y.; Birdsey, R.A.; Fang, J.; Houghton, R.; Kauppi, P.E.; Kurz, W.A.; Phillips, O.L.; Shvidenko, A.; Lewis, S.L.; Canadell, J.G.; et al. A Large and Persistent Carbon Sink in the World's Forests. *Science (1979).* **2011**, *333*, 988–993, doi:10.1126/science.1201609.
7. Phillips, O.L. The Changing Ecology of Tropical Forests. *Biodivers. Conserv.* **1997**, *6*, 291–311, doi:10.1023/A:1018352405482.
8. Lewis, S.L. Tropical Forests and the Changing Earth System. *Philosophical Transactions of the Royal Society B: Biological Sciences* 2006, *361*, 195–210.
9. Putz, F.E.; Redford, K.H. The Importance of Defining "Forest": Tropical Forest Degradation, Deforestation, Long-Term Phase Shifts, and Further Transitions. *Biotropica* **2010**, *42*, 10–20, doi:10.1111/j.1744-7429.2009.00567.x.
10. Mitchard, E.T.A. The Tropical Forest Carbon Cycle and Climate Change. *Nature* **2018**, *559*, 527–534, doi:10.1038/s41586-018-0300-2.
11. Duncanson, L.; Disney, M.; Armston, J.; Nickeson, J.; Minor, D. Committee on Earth Observation Satellites Working Group on Calibration and Validation Land Product Validation Subgroup Aboveground Woody Biomass Product Validation Good Practices Protocol. *Good Practices for Satellite Derived Land Product Validation* **2021**, 0–236, doi:10.5067/doc/ceoswgcv/lpv/agb.001.
12. Brown, S.; Gillespie, A.J.R.; Lugo, A.E. Estimation Methods for Tropical Forests.Pdf 1989, *35*, 881–902.
13. Chave, J.; Andalo, C.; Brown, S.; Cairns, M.A.; Chambers, J.Q.; Eamus, D.; Fölster, H.; Fromard, F.; Higuchi, N.; Kira, T.; et al. Tree Allometry and Improved Estimation of Carbon Stocks and Balance in Tropical Forests. *Oecologia* **2005**, *145*, 87–99, doi:10.1007/s00442-005-0100-x.
14. Chave, J.; Réjou-Méchain, M.; Búrquez, A.; Chidumayo, E.; Colgan, M.S.; Delitti, W.B.C.; Duque, A.; Eid, T.; Fearnside, P.M.; Goodman, R.C.; et al. Improved Allometric Models to Estimate the Aboveground Biomass of Tropical Trees. *Glob. Chang. Biol.* **2014**, *20*, 3177–3190, doi:10.1111/gcb.12629.
15. Chave, J. Tree Height Measurement Protocol – J Chave Measuring Tree Height for Tropical Forest Trees A Field Manual for the CTFS Sites. **2005**.
16. Fayolle, A.; Ngomanda, A.; Mbasi, M.; Barbier, N.; Bocko, Y.; Boyemba, F.; Couteron, P.; Fonton, N.; Kamdem, N.; Katembo, J.; et al. A Regional Allometry for the Congo Basin Forests Based on the Largest Ever Destructive Sampling. *For. Ecol. Manage.* **2018**, *430*, 228–240, doi:10.1016/j.foreco.2018.07.030.
17. Ngomanda, A.; Engone Obiang, N.L.; Lebamba, J.; Moundounga Mavouroulou, Q.; Gomat, H.; Mankou, G.S.; Loumeto, J.; Midoko Iponga, D.; Kossi Ditsouga, F.; Zinga Koumba, R.; et al. Site-Specific versus Pantropical Allometric Equations: Which Option to Estimate the Biomass of a Moist Central African Forest? *For. Ecol. Manage.* **2014**, *312*, 1–9, doi:10.1016/j.foreco.2013.10.029.
18. Dorisca, S.; Durrieur, M.D.L.; Fontez, B.; Giraud, A.; Riera, B. Équations Entre Le Diamètre Et Le Volume Total. *Bois et Forêts des Tropiques* **2011**, *308*, 87–95.
19. Djomo, A.N.; Chimi, C.D. Tree Allometric Equations for Estimation of above, below and Total Biomass in a Tropical Moist Forest: Case Study with Application to Remote Sensing. *For. Ecol. Manage.* **2017**, *391*, 184–193, doi:10.1016/j.foreco.2017.02.022.
20. Molto, Q.; Hérault, B.; Boreux, J.J.; Daullet, M.; Rousteau, A.; Rossi, V. Predicting Tree Heights for Biomass Estimates in Tropical Forests -A Test from French Guiana. *Biogeosciences* **2014**, *11*, 3121–3130, doi:10.5194/bg-11-3121-2014.

 doi:10.20944/preprints202603.1717.v2

21. Goodman, R.C.; Phillips, O.L.; Baker, T.R. The Importance of Crown Dimensions to Improve Tropical Tree Biomass Estimates. *Ecological Applications* **2014**, *24*, 680–698, doi:10.1890/13-0070.1.
22. Ploton, P.; Barbier, N.; Momo, S.T.; Rejou-Mechain, M.; Boyemba Bosela, F.; Chuyong, G.; Dauby, G.; Droissart, V.; Fayolle, A.; Calisto Goodman, R.; et al. Closing a Gap in Tropical Forest Biomass Estimation: Taking Crown Mass Variation into Account in Pantropical Allometries. *Biogeosciences* **2016**, *13*, 1571–1585, doi:10.5194/bg-13-1571-2016.
23. Feldpausch, T.R.; Lloyd, J.; Lewis, S.L.; Brienen, R.J.W.; Gloor, M.; Monteagudo Mendoza, A.; Lopez-Gonzalez, G.; Banin, L.; Abu Salim, K.; Affum-Baffoe, K.; et al. Tree Height Integrated into Pantropical Forest Biomass Estimates. *Biogeosciences* **2012**, *9*, 3381–3403, doi:10.5194/bg-9-3381-2012.
24. Jucker, T.; Caspersen, J.; Chave, J.; Antin, C.; Barbier, N.; Bongers, F.; Dalponte, M.; van Ewijk, K.Y.; Forrester, D.I.; Haeni, M.; et al. Allometric Equations for Integrating Remote Sensing Imagery into Forest Monitoring Programmes. *Glob. Chang. Biol.* **2017**, *23*, 177–190, doi:10.1111/gcb.13388.
25. Hess, C.; Bienert, A.; Härdtle, W.; Von Oheimb, G. Does Tree Architectural Complexity Influence the Accuracy of Wood Volume Estimates of Single Young Trees by Terrestrial Laser Scanning? *Forests 2015, Vol. 6, Pages 3847-3867* **2015**, *6*, 3847–3867, doi:10.3390/F6113847.
26. Lines, E.R.; Fischer, F.J.; Owen, H.J.F.; Jucker, T. The Shape of Trees: Reimagining Forest Ecology in Three Dimensions with Remote Sensing. *Journal of Ecology* **2022**, 1–16, doi:10.1111/1365-2745.13944.
27. Disney, M. Terrestrial LiDAR: A Three-Dimensional Revolution in How We Look at Trees. *New Phytologist* **2019**, *222*, 1736–1741, doi:10.1111/NPH.15517.
28. Terryn, L.; Calders, K.; Åkerblom, M.; Bartholomeus, H.; Disney, M.; Levick, S.; Origo, N.; Raumonen, P.; Verbeeck, H. Analysing Individual 3D Tree Structure Using the R Package ITSMe. *Methods Ecol. Evol.* **2023**, *14*, 231–241, doi:10.1111/2041-210X.14026.
29. Raumonen, P.; Kaasalainen, M.; Åkerblom, M.; Kaasalainen, S.; Kaartinen, H.; Vastaranta, M.; Holopainen, M.; Disney, M.; Lewis, P. Fast Automatic Precision Tree Models from Terrestrial Laser Scanner Data. *Remote Sens. (Basel).* **2013**, *5*, 491–520, doi:10.3390/rs5020491.
30. Verbeeck, H.; Bauters, M.; Jackson, T.; Shenkin, A.; Disney, M.; Calders, K. Time for a Plant Structural Economics Spectrum. *Frontiers in Forests and Global Change* **2019**, *2*, 1–5, doi:10.3389/ffgc.2019.00043.
31. Åkerblom, M.; Raumonen, P.; Mäkipää, R.; Kaasalainen, M. Automatic Tree Species Recognition with Quantitative Structure Models. *Remote Sens. Environ.* **2017**, *191*, 1–12, doi:10.1016/j.rse.2016.12.002.
32. Hackenberg, J.; Spiecker, H.; Calders, K.; Disney, M.; Raumonen, P. SimpleTree - An Efficient Open Source Tool to Build Tree Models from TLS Clouds. *Forests* **2015**, *6*, 4245–4294, doi:10.3390/f6114245.
33. Kaasalainen, S.; Krooks, A.; Liski, J.; Raumonen, P.; Kaartinen, H.; Kaasalainen, M.; Puttonen, E.; Anttila, K.; Mäkipää, R.; Kaasalainen, S.; et al. Change Detection of Tree Biomass with Terrestrial Laser Scanning and Quantitative Structure Modelling. *Remote Sens. (Basel).* **2014**, *6*, 3906–3922, doi:10.3390/rs6053906.
34. Burt, A.; Disney, M.; Calders, K. Extracting Individual Trees from Lidar Point Clouds Using Treeseg. *Methods Ecol. Evol.* **2019**, *10*, 438–445, doi:10.1111/2041-210X.13121.
35. Raumonen, P.; Kaasalainen, S.; Kaasalainen, M.; Kaartinen, H. Approximation of Volume and Branch Size Distribution of Trees From Laser Scanner Data. *ISPRS - International Archives of the Photogrammetry, Remote Sensing and Spatial Information Sciences* **2012**, *XXXVIII-5/*, 79–84, doi:10.5194/isprsarchives-XXXVIII-5-W12-79-2011.
36. Raumonen, P.; Casella, E.; Calders, K.; Murphy, S.; Åkerbloma, M.; Kaasalainen, M. Massive-Scale Tree Modelling From Tls Data. *ISPRS Annals of Photogrammetry, Remote Sensing and Spatial Information Sciences* **2015**, *II-3/W4*, 189–196, doi:10.5194/isprsannals-II-3-W4-189-2015.
37. Disney, M.; Burt, A.; Calders, K.; Schaaf, C.; Stovall, A. Innovations in Ground and Airborne Technologies as Reference and for Training and Validation: Terrestrial Laser Scanning (TLS). *Surv. Geophys.* **2019**, *40*, 937–958, doi:10.1007/s10712-019-09527-x.
38. Calders, K.; Newnham, G.; Burt, A.; Murphy, S.; Raumonen, P.; Herold, M.; Culvenor, D.; Avitabile, V.; Disney, M.; Armston, J.; et al. Nondestructive Estimates of Above-Ground Biomass Using Terrestrial Laser Scanning. *Methods Ecol. Evol.* **2015**, *6*, 198–208, doi:10.1111/2041-210X.12301.
39. Momo Takoudjou, S.; Ploton, P.; Sonké, B.; Hackenberg, J.; Griffon, S.; de Coligny, F.; Kamdem, N.G.; Libalah, M.; Mofack, G.; Le Moguédec, G.; et al. Using Terrestrial Laser Scanning Data to Estimate Large

 doi:10.20944/preprints202603.1717.v2

Tropical Trees Biomass and Calibrate Allometric Models: A Comparison with Traditional Destructive Approach. *Methods Ecol. Evol.* **2018**, *9*, 905–916, doi:10.1111/2041-210X.12933.

40. Lau, A.; Calders, K.; Bartholomeus, H.; Martius, C.; Raumonen, P.; Herold, M.; Vicari, M.; Sukhdeo, H.; Singh, J.; Goodman, R.C. Tree Biomass Equations from Terrestrial LiDAR: A Case Study in Guyana. *Forests* **2019**, *10*, 1–18, doi:10.3390/f10060527.
41. Gonzalez de Tanago, J.; Lau, A.; Bartholomeus, H.; Herold, M.; Avitabile, V.; Raumonen, P.; Martius, C.; Goodman, R.C.; Disney, M.; Manuri, S.; et al. Estimation of Above-Ground Biomass of Large Tropical Trees with Terrestrial LiDAR. *Methods Ecol. Evol.* **2018**, *9*, 223–234, doi:10.1111/2041-210X.12904.
42. Demol, M.; Verbeeck, H.; Gielen, B.; Armston, J.; Burt, A.; Disney, M.; Duncanson, L.; Hackenberg, J.; Kükenbrink, D.; Lau, A.; et al. Estimating Forest Above-Ground Biomass with Terrestrial Laser Scanning: Current Status and Future Directions. *Methods Ecol. Evol.* **2022**, *13*, 1628–1639, doi:10.1111/2041-210X.13906.
43. Vandendaele, B.; Martin-Ducup, O.; Fournier, R.A.; Pelletier, G. Evaluation of Mobile Laser Scanning Acquisition Scenarios for Automated Wood Volume Estimation in a Temperate Hardwood Forest Using Quantitative Structural Models. *Canadian Journal of Forest Research* **2024**, doi:10.1139/cjfr-2023-0202.
44. Duncanson, L.; Disney, M.; Armston, J.; Nickeson, J.; Minor, D. Committee on Earth Observation Satellites Working Group on Calibration and Validation Land Product Validation Subgroup Aboveground Woody Biomass Product Validation Good Practices Protocol. *Good Practices for Satellite Derived Land Product Validation* **2021**, 0–236, doi:10.5067/doc/ceoswgcv/lpv/agb.001.
45. Sagang, L.B.T.; Favrichon, S.; Dalagnol, R.; Ordway, E.M.; Medjibe, V.; Manfoumbi, F.; Obame, C.; Wagner, F.; George-Chacon, S.; White, L.; et al. Unveiling Spatial Variations of High Forest Live Biomass Carbon Stocks of Gabon Using Advanced Remote Sensing Techniques. *Environmental Research Letters* **2024**, *19*, 74038, doi:10.1088/1748-9326/ad5572.
46. Kossi Ditsouga, A.F.; Moundounga Mavouroulou, Q.; Moundounga, C.G.; Fayolle, A.; Picard, N.; Sato, A.; Ngomanda, A. Tree Belowground Biomass in Congo Basin Forests: Allometric Equations and Scaling with Aboveground Biomass. *Forestry: An International Journal of Forest Research* **2024**, 1–10, doi:10.1093/forestry/cpae009.
47. Salis, S.M.; Assis, M.A.; Mattos, P.P.; Pião, A.C.S. Estimating the Aboveground Biomass and Wood Volume of Savanna Woodlands in Brazil's Pantanal Wetlands Based on Allometric Correlations. *For. Ecol. Manage.* **2006**, *228*, 61–68, doi:10.1016/j.foreco.2006.02.025.
48. Kenzo, T.; Ichie, T.; Hattori, D.; Kendawang, J.J.; Sakurai, K.; Ninomiya, I. Changes in Above- and Belowground Biomass in Early Successional Tropical Secondary Forests after Shifting Cultivation in Sarawak, Malaysia. *For. Ecol. Manage.* **2010**, *260*, 875–882, doi:10.1016/j.foreco.2010.06.006.
49. Vicari, M.B.; Disney, M.; Wilkes, P.; Burt, A.; Calders, K.; Woodgate, W. Leaf and Wood Classification Framework for Terrestrial LiDAR Point Clouds. *Methods Ecol. Evol.* **2019**, *10*, 680–694, doi:10.1111/2041-210X.13144.
50. Wang, D.; Momo Takoudjou, S.; Casella, E. LeWoS: A Universal Leaf-Wood Classification Method to Facilitate the 3D Modelling of Large Tropical Trees Using Terrestrial LiDAR. *Methods Ecol. Evol.* **2020**, *11*, 376–389, doi:10.1111/2041-210X.13342.
51. Osnas, J.L.D.; Lichstein, J.W.; Reich, P.B.; Pacala, S.W. Global Leaf Trait Relationships: Mass, Area, and the Leaf Economics Spectrum. *Science (1979).* **2013**, *340*, 741–744, doi:10.1126/science.1231574.
52. Díaz, S.; Kattge, J.; Cornelissen, J.H.C.; Wright, I.J.; Lavorel, S.; Dray, S.; Reu, B.; Kleyer, M.; Wirth, C.; Colin Prentice, I.; et al. The Global Spectrum of Plant Form and Function. *Nature* **2016**, *529*, 167–171, doi:10.1038/nature16489.
53. Wright, I.J.; Reich, P.B.; Westoby, M.; Ackerly, D.D.; Baruch, Z.; Bongers, F.; Cavender-Bares, J.; Chapin, T.; Cornellssen, J.H.C.; Diemer, M.; et al. The Worldwide Leaf Economics Spectrum. *Nature* **2004**, *428*, 821–827, doi:10.1038/nature02403.
54. Jucker, T.; Fischer, F.J.; Chave, J.; Coomes, D.A.; Caspersen, J.; Ali, A.; Loubota Panzou, G.J.; Feldpausch, T.R.; Falster, D.; Usoltsev, V.A.; et al. Tallo: A Global Tree Allometry and Crown Architecture Database. *Glob. Chang. Biol.* **2022**, *28*, 5254–5268, doi:10.1111/gcb.16302.

 doi:10.20944/preprints202603.1717.v2

55. Jackson, T.; Shenkin, A.; Moore, J.; Bunce, A.; Van Emmerik, T.; Kane, B.; Burcham, D.; James, K.; Selker, J.; Calders, K.; et al. An Architectural Understanding of Natural Sway Frequencies in Trees. *J. R. Soc. Interface* **2019**, *16*, doi:10.1098/rsif.2019.0116.
56. Jucker, T.; Fischer, F.J.; Chave, J.; Coomes, D.A.; Caspersen, J.; Ali, A.; Loubota Panzou, G.J.; Feldpausch, T.R.; Falster, D.; Usoltsev, V.A.; et al. The Global Spectrum of Tree Crown Architecture. *Nature Communications* **2025**, *16*, 45–50, doi:10.1038/s41467-025-60262-x.
57. Fischer, F.J.; Morgan, B.; Jackson, T.; Chave, J.; Coomes, D.; Cushman, K.; Dalagnol, R.; Dalponte, M.; Duncanson, L.; Saatchi, S.; et al. The Global Canopy Atlas: Analysis-Ready Maps of 3D Structure for the World's Woody Ecosystems. *bioRxiv* **2025**, 2025.08.31.673375, doi:10.1101/2025.08.31.673375.
58. White, F. *The Vegetation of Africa*; 1983;
59. Droissart, V.; Verlynde, S.; Ramandimbisoa, B.; Andriamahefarivo, L.; Stévart, T. Diversity and Distribution of Orchidaceae in One of the World's Most Threatened Plant Hotspots (Madagascar). *Biodivers. Data J.* **2023**, *11*, e106223, doi:10.3897/BDJ.11.E106223.
60. Fayolle, A.; Doucet, J.L.; Gillet, J.F.; Bourland, N.; Lejeune, P. Tree Allometry in Central Africa: Testing the Validity of Pantropical Multi-Species Allometric Equations for Estimating Biomass and Carbon Stocks. *For. Ecol. Manage.* **2013**, *305*, 29–37, doi:10.1016/j.foreco.2013.05.036.
61. Jones, A.; Breuning-Madsen, H.; Brossard, M.; Dampha, A.; Deckers, J.; Dewitte, O.; Kilasara, M. *Soil Atlas of Africa (Luxembourg: European Commission, Publications Office of the European Union).*; 2013;
62. Doucet, J.L.; Daïnou, K.; Ligot, G.; Ouédraogo, D.Y.; Bourland, N.; Ward, S.E.; Tekam, P.; Lagoute, P.; Fayolle, A. Enrichment of Central African Logged Forests with High-Value Tree Species: Testing a New Approach to Regenerating Degraded Forests. *Int. J. Biodivers. Sci. Ecosyst. Serv. Manag.* **2016**, *12*, 83–95, doi:10.1080/21513732.2016.1168868.
63. Proulx, H.; Jacobs, J.M.; Burakowski, E.A.; Cho, E.; Hunsaker, A.G.; Sullivan, F.B.; Palace, M.; Wagner, C. Comparison of In-Situ Snow Depth Measurements and Impacts on Validation of Unpiloted Aerial System Lidar over a Mixed-Use Temperate Forest Landscape. **2022**, doi:10.5194/TC-2022-7.
64. Bauwens, S.; Bartholomeus, H.; Calders, K.; Lejeune, P. Forest Inventory with Terrestrial LiDAR: A Comparison of Static and Hand-Held Mobile Laser Scanning. *Forests* **2016**, *7*, 127, doi:10.3390/f7060127.
65. Vandendaele, B.; Martin-Ducup, O.; Fournier, R.A.; Pelletier, G.; Lejeune, P. Mobile Laser Scanning for Estimating Tree Structural Attributes in a Temperate Hardwood Forest. *Remote Sens. (Basel).* **2022**, *14*, 4522, doi:10.3390/RS14184522.
66. Zanne, A.E.; Lopez-Gonzalez, G.; Coomes, D.A.A.; Ilic, J.; Jansen, S.; Lewis, S.L.S.L.; Miller, R.B.B.; Swenson, N.G.G.; Wiemann, M.C.C.; Chave, J. Data from: Towards a Worldwide Wood Economics Spectrum. Dryad Digital Repository. *Dryad* 2009, *235*, 33.
67. Réjou-Méchain, M.; Tanguy, A.; Piponiot, C.; Chave, J.; Hérault, B. Biomass: An R Package for Estimating Above-Ground Biomass and Its Uncertainty in Tropical Forests. *Methods Ecol. Evol.* **2017**, *8*, 1163–1167, doi:10.1111/2041-210X.12753.
68. Sirri, N.F.; Libalah, M.B.; Momo Takoudjou, S.; Ploton, P.; Medjibe, V.; Kamdem, N.G.; Mofack, G.; Sonké, B.; Barbier, N. Allometric Models to Estimate Leaf Area for Tropical African Broadleaved Forests. *Geophys. Res. Lett.* **2019**, *46*, 8985–8994, doi:10.1029/2019GL083514.
69. Martin-Ducup, O.; Mofack, G.; Wang, D.; Raumonen, P.; Ploton, P.; Sonké, B.; Barbier, N.; Couteron, P.; Pélissier, R. Evaluation of Automated Pipelines for Tree and Plot Metric Estimation from TLS Data in Tropical Forest Areas. *Ann. Bot.* **2021**, *128*, 753–766, doi:10.1093/aob/mcab051.
70. Momo, S.T.; Ploton, P.; Martin-Ducup, O.; Lehnebach, R.; Fortunel, C.; Sagang, L.B.T.; Boyemba, F.; Couteron, P.; Fayolle, A.; Libalah, M.; et al. Leveraging Signatures of Plant Functional Strategies in Wood Density Profiles of African Trees to Correct Mass Estimations From Terrestrial Laser Data. *Sci. Rep.* **2020**, *10*, 1–11, doi:10.1038/s41598-020-58733-w.
71. R Core Team A Language and Environment for Statistical Computing 2025.
72. Poorter, H.; Jagodzinski, A.M.; Ruiz-peinado, R.; Kuyah, S.; Luo, Y.; Oleksyn, J.; Usoltsev, V.A.; Buckley, T.N.; Reich, P.B.; Sack, L. How Does Biomass Distribution Change with Size and Differ among Species ? An Analysis for 1200 Plant Species from Five Continents. **2015**.

 doi:10.20944/preprints202603.1717.v2

73. Jensen, J. Linking Tree Species Diversity , Productivity , and Carbon Sequestration in Mixed-Species Forest Plantations From Patterns to Mechanisms Linking Tree Species Diversity , Productivity , and Carbon Sequestration, SWEDISH UNIVERSITY OF AGRICULTURAL SCIENCES : SLU, 2025.
74. Gonzalez de Tanago, J.M.; Lau, A.; Bartholomeusm, H.; Herold, M.; Valerio, A.; Raumonen, P.; Martius, C.; Goodman, R.; Disney, M.; Manuri, S.; et al. Estimation of above -Ground Biomass of Large Tropical Trees with Terrestrial LiDARof Results Obtained in the DULCIS Study. **2017**, doi:DOI: 10.1111/2041-210X.12904.
75. Lau, A.; Martius, C.; Bartholomeus, H.; Shenkin, A.; Jackson, T.; Malhi, Y.; Herold, M.; Bentley, L.P. Estimating Architecture-Based Metabolic Scaling Exponents of Tropical Trees Using Terrestrial LiDAR and 3D Modelling. *For. Ecol. Manage.* **2019**, *439*, 132–145, doi:10.1016/j.foreco.2019.02.019.
76. Banin, L.; Feldpausch, T.R.; Phillips, O.L.; Baker, T.R.; Lloyd, J.; Affum-Baffoe, K.; Arets, E.J.M.M.; Berry, N.J.; Bradford, M.; Brienen, R.J.W.; et al. What Controls Tropical Forest Architecture? Testing Environmental, Structural and Floristic Drivers. *Global Ecology and Biogeography* **2012**, *21*, 1179–1190, doi:10.1111/j.1466-8238.2012.00778.x.
77. Vicari, M.B.; Pisek, J.; Disney, M. New Estimates of Leaf Angle Distribution from Terrestrial LiDAR: Comparison with Measured and Modelled Estimates from Nine Broadleaf Tree Species. *Agric. For. Meteorol.* **2019**, *264*, 322–333, doi:10.1016/J.AGRFORMET.2018.10.021.
78. Malhi, Y.; Jackson, T.; Bentley, L.P.; Lau, A.; Shenkin, A.; Herold, M.; Calders, K.; Bartholomeus, H.; Disney, M.I. New Perspectives on the Ecology of Tree Structure and Tree Communities through Terrestrial Laser Scanning. *Interface Focus* **2018**, *8*, 2015–2017, doi:10.1098/rsfs.2017.0052.
79. Blanchard, E.; Birnbaum, P.; Ibanez, T.; Boutreux, T.; Antin, C.; Ploton, P.; Vincent, G.; Pouteau, R.; Vandrot, H.; Hequet, V.; et al. Contrasted Allometries between Stem Diameter, Crown Area, and Tree Height in Five Tropical Biogeographic Areas. *Trees - Structure and Function* **2016**, *30*, 1953–1968, doi:10.1007/S00468-016-1424-3.
80. Schepaschenko, D.; Chave, J.; Phillips, O.L.; Lewis, S.L.; Davies, S.J.; Réjou-Méchain, M.; Sist, P.; Scipal, K.; Perger, C.; Herault, B.; et al. The Forest Observation System, Building a Global Reference Dataset for Remote Sensing of Forest Biomass. *Sci. Data* **2019**, *6*, 1–11, doi:10.1038/s41597-019-0196-1.